SCIENTIFIC REPORTS
nature research

OPEN

Towards integrated metatronics: a holistic approach on precise optical and electrical properties of Indium Tin Oxide

Received: 11 January 2019
Accepted: 15 July 2019
Published online: 02 August 2019

Yaliang Gui[1], Mario Miscuglio[1], Zhizhen Ma[1], Mohammad H. Tahersima[1], Shuai Sun[1], Rubab Amin[1], Hamed Dalir[2] & Volker J. Sorger[1]

The class of transparent conductive oxides includes the material indium tin oxide (ITO) and has become a widely used material of modern every-day life such as in touch screens of smart phones and watches, but also used as an optically transparent low electrically-resistive contract in the photovoltaics industry. More recently ITO has shown epsilon-near-zero (ENZ) behavior in the telecommunication frequency band enabling both strong index modulation and other optically-exotic applications such as metatronics. However, the ability to precisely obtain targeted electrical and optical material properties in ITO is still challenging due to complex intrinsic effects in ITO and as such no integrated metatronic platform has been demonstrated to-date. Here we deliver an extensive and accurate description process parameter of RF-sputtering, showing a holistic control of the quality of ITO thin films in the visible and particularly near-infrared spectral region. We are able to custom-engineer the ENZ point across the telecommunication band by explicitly controlling the sputtering process conditions. Exploiting this control, we design a functional sub-wavelength-scale filter based on lumped circuit-elements, towards the realization of integrated metatronic devices and circuits.

Indium Tin Oxide films have been extensively employed for diverse applications in the fields of optics and electronics in both research and industry[1]. Multiple uses of ITO range from photovoltaics[2–5] to conductive displays[6], integrated photonics[7,8] and solid-state[9]. ITO's versatility can be attributed to its concurrent optical transparency (T) and sheet resistance (R_{sheet}) (Figure of merit = T/R_{sheet})[10], as well as compatibility with the established technology[11]. Moreover, ITO's carrier density can be electrostatically tuned similarly to metal-oxide-semiconductor (MOS) capacitors, simply by applying a bias voltage. This carrier modulation translates into either a refractive index or absorption change[12]. For this reason, ITO has been largely employed as an active material in electro-optic modulators[13–20] in integrated photonics and plasmonic metasurfaces[21–24], specifically displaying high performance optical electro-refractive modulation[25]. In this regard, recently, new possibilities are emerging to use ITO as an active material in sub-wavelength waveguide integrated electro-optic modulators, which showed high performances regarding extinction ratio dB/μm[7,26–28]. Nevertheless, according to the application, the fundamental challenge in processing ITO is concurrently obtaining thin films with favorable electrical and optical conditions. For instance, to design efficient, transparent conductors for photovoltaic and conductive display applications, relatively low resistivity and optical transparency have to be achieved. For electro-optic applications, the wavelength of the epsilon-near-zero (ENZ) point, the carrier concentration and absorption losses, which define the modulation strength, need to be accounted for. Moreover, ITO films could enable an ENZ circuit board and nanoscale structured ITO RCL-equivalent circuit elements, thus creating a viable means to realize metatronic circuits[29]. Recently[30], ITO films have exhibited an extremely large ultrafast third-order nonlinearity at ENZ wavelengths, which could be exploited in nonlinear nano-optics applications. Therefore, control over ENZ wavelength could constitute a fundamental building block towards the realization of metatronic devices[31] as well as nonlinear optical components. However, ITO's material parameters such as resistivity and permittivity are complex depending on a multitude of process conditions. For this reason, obtaining a thorough understanding of the effects of

[1]Department of Electrical and Computer Engineering, George Washington University, 800 22nd St. NW, Washington, DC, 20052, USA. [2]Omega Optics, Inc. 8500 Shoal Creek Blvd., Bldg. 4, Suite 200, Austin, Texas, 78757, USA. Correspondence and requests for materials should be addressed to V.J.S. (email: sorger@gwu.edu)

specific process parameters to the electro-optic properties of the ITO films is highly desirable and still represents an open challenge. Recently system parameters on different deposition techniques such as Plasma-Enhanced Metal-Organic Chemical Vapor Deposition (PEMOCVD)[32], Ion Beam Assisted Deposition (IBAD)[33] and DC sputtering[34,35] have been developed in an ad-hoc manner, however a significantly cross-validation process for the RF sputtering process and subsequent thermal treatment is still lacking. While previous work investigated selected material properties[36–40], a holistic understanding of a) the inter relationship among these material parameters and b) the precise process control thereof is far from being completely understood. In addition, a viable path to realize metatronic circuits offering the best of both photonic signal communication and nanoscale component density is yet outstanding. Here we show the holistic control of the quality of ITO thin films in the visible and particularly near-infrared spectral region. We alter key material-film property factors during a RF-sputtering process such as the oxygen concentration and thermal annealing. Using this approach, we thence develop an interdependently-complete set of metrology processes for determining the conductivity, carrier density, and mobility of these ITO films and bring them in congruence with values obtained from spectroscopic ellipsometry. We discover a cross-sectional film thickness-dependent carrier distribution as a function of thermal carrier activation and demonstrate ability to tune the resistivity gradient by restoring the film crystalline structure upon thermal treatment. Moreover, the ultimate aim in our work is not simply characterizing the film optical and electrical properties, which to a certain extent has been reported in[36–39] for RF-sputtered films, but also to provide specific guidelines to other research groups and engineers in the selection of process parameters required to fabricate optimized optical modules based on ITO for integrated photonics and plasmonics. It is indeed essential when fabricating ITO-based active optical component to hand-pick the process parameters, which provides favorable initial material conditions (without applying any bias), such as proximity to ENZ or damping, to optimize the device figure of merits, such as insertion losses (IL), extinction ratio (ER), device length (L) and bias required for modulation (e.g. V_π).

We further demonstrate the precise control over ENZ film properties across the telecommunication band, which enables engineering a variety of optoelectronic devices with exotic properties. Using this process control in ITO, we analyze a functional sub-wavelength-scale filter based on lumped circuit-elements in a metatronic approach. Such self-consistent process and precise control of ITO's properties electrical, spectral, and optical parameters serves a wide application space such as in optoelectronics, metamaterials, metatronics, quantum technologies, energy-harvesting, and sensing.

ITO Deposition and Characterization: Validation Process

We initially focus on defining a consistent and tunable ITO deposition process using RF sputtering, which allows to finely adjust the electrical and optical properties of the film. The purpose of our study is ultimately to engineer ITO film properties to deliver well-defined control over critical parameters for obtaining films that could enhance fabricated device properties.

In our experiments, films are deposited on $1 \times 1\,cm^2$ Si/SiO_2 substrates, utilizing reactive RF sputtering (Denton Vacuum Discovery 550 Sputtering System). ITO sputtering targets consist of 10% SnO_2 to 90% In_2O_3 by weight (refer to the method section for details). Several replicated samples are produced for each oxygen flow-rate condition (0, 5, 10, 20, 30 sccm) and sputtering time (500,1000,1500,2000 s), for 40 sccm Argon flow-rate (50 sccm Ar flow rate study is presented in SI). For each condition, represented by a single data-point, the study is repeated four times for statistical purpose and repeatability. Conducive to promote crystallinity and study the charge carrier activation mechanisms, a sub-group of deposited films is subjected to a thermal treatment at 350 °C in the inert atmosphere (a mixture of H_2 and N_2) for 15 minutes. Contrary to atmosphere annealing treatment[41], which aims to promote optical transmittance by filling vacancies, an annealing treatment in inert conditions improves both the film conductivity[42,43]. Differently from other studies[32–35,44], hereby we map the overall conductivity and optical absorption variation for different oxygen flow rates and deposition time. After deposition, the step height of ITO films is measured in multiple areas for estimating the uniformity of the deposition and determining the initial fitting parameters in our spectroscopic ellipsometry.

For assessing the quality of our process and determining its reliability, direct and indirect measurements are used as rigorous cross validation tools. The resistivity of the thin film is indirectly obtained via ellipsometry and, directly, through 4-probe station (Four Dimensions 280DI) and Hall effect measurement system (HMS-5500). Hall measurement also gives information on the carrier type (n-doped), concentration and mobility.

A straightforward Drude model, as well as the material model provided by Genosc library, is inaccurate, leaving aside a complete optical description of the film in the wide spectral window considered, under these process conditions. Relating to this, we use a fitting sequence, which includes Cauchy, B-spline, Drude and Lorentz models[42], allowing inter alia, an accurate description of the electrooptical features of the film as function of its depth (see SI). This rigorous model for fitting the optical spectra enables the description of the refractive index and optical conductivity, as well as mobility and carrier concentration, which is cross-validated by hall bar and 4-probe direct *in-situ* measurements (Fig. 1b). The ENZ position is evaluated from the complex permittivity by ellipsometry.

Effects of the Oxygen Flow Rate and Thermal Treatment on Dispersion and Absorption

To establish baselines control over ITO films, we aim to understand the thickness-related influence on material parameters. We find that thinner films are obtained for higher oxygen concentration because of reduced sputter material deposition rate (Fig. 2a). Quantitatively, we find that for a fixed deposition time (e.g. 1500 s shown in S1 in SI) the ITO film thickness decreases by: $t = ae^{bx}$ being t the thickness, a = 509 nm the y-intercept and b = 0.047sccm the decay constant (RMS 97%). Oxygen flow rate can affect the mean free path and gas current of null ion, which will lead to a different deposition rate. Thus the, thickness for a given deposition time would

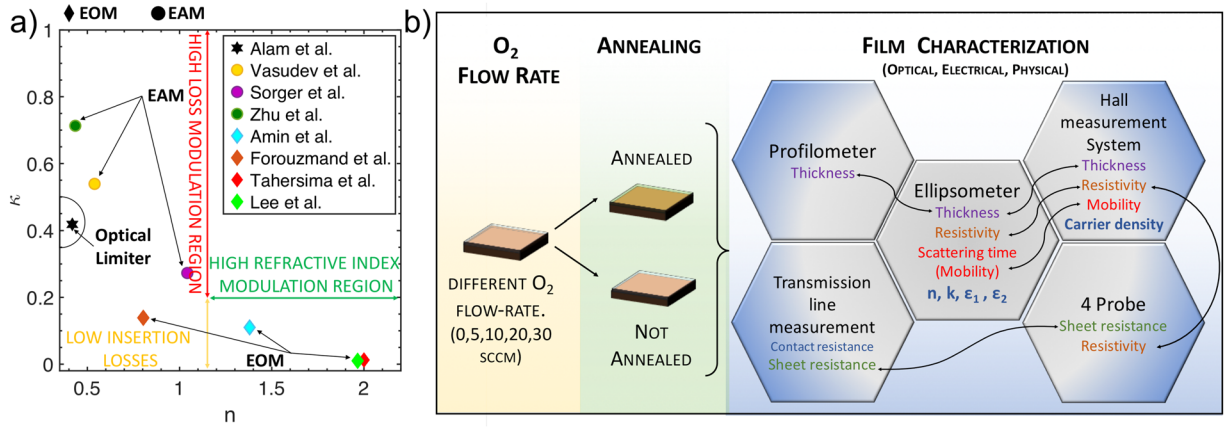

Figure 1. (**a**) Experimental and theoretical complex refractive index of the state-of-the-art ITO based electro-refractive phase and absorption modulators in integrated photonics (EOM: Amin *et al.*[25] and Tahersima *et al.*[51]; EAM: Sorger *et al.*[13], Vasudev *et al.*[15] and Zhu[55]) and plasmonics (Lee *et al.*[22] and Forouzmand *et al.*[48]) in their light off-state (examplary context: EO modulators). Also, ITO based Optical limiter (Alam *et al.*[30]) in the light off state is reported. Region of high loss (red arrow) and refractive index (green arrow) modulation are highlighted. (**b**) Flow chart of the ITO film process and holistic characterization. Different films are sputtered at different Oxygen flow-rate conditions (0, 5, 10, 20, 30 sccm). Post annealing process in a sealed chamber in inert atmosphere (H_2 and N_2). Thickness is directly measured through profilometer. Validation of the electro-optic properties of ITO films through complimentary set-ups which includes Hall, 4-Probe and Transmission line measurements. The black arrows illustrate the cross-validation mechanisms opted in this study.

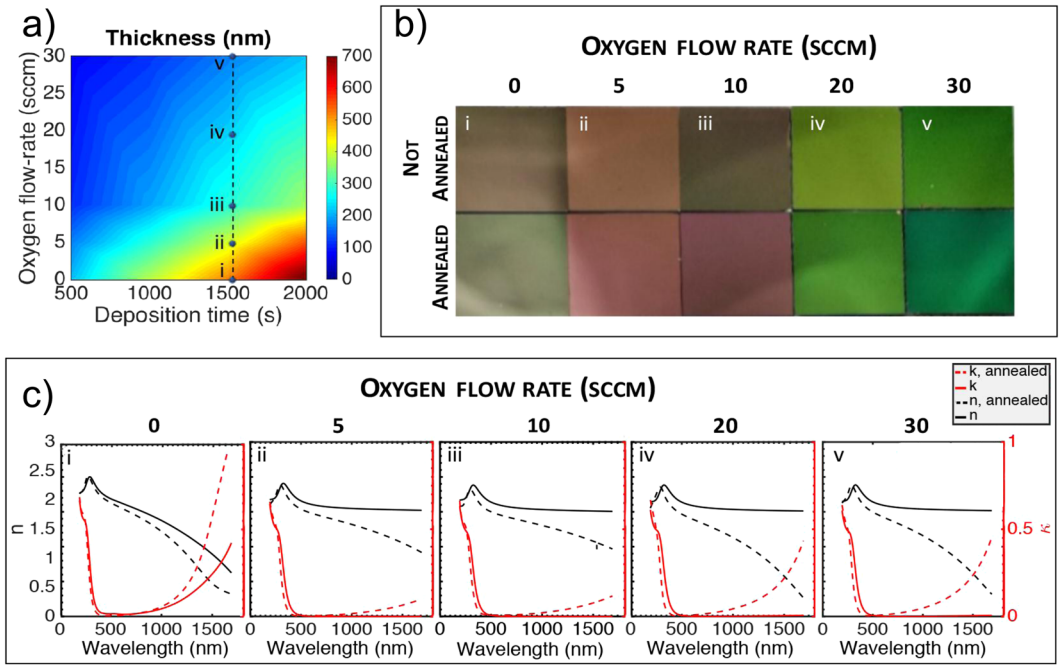

Figure 2. Oxygen flow-rate and post deposition heating (annealing, 350 °C, 15 minutes, see SI) treatment effects: (**a**) ITO film Thickness as function of the Oxygen flow-rate (0, 5, 10, 20, 30) for different deposition time (500 s, 1000 s, 1500 s, 2000 s). (**b**) Images of the 1 × 1 cm^2 ITO films on SiO_2/Si substrate for the different oxygen flow-rate, before and after annealing. (**c**) Spectral behavior of the real (black) and imaginary (red) part of the refractive index of films sputtered using different oxygen flow-rate and effects of the post-deposition heat treatment process (dashed lines).

decrease with the oxygen flow rate[45]. The deposition conditions, summarized in the method section, enable a precise control of the thickness, with a repeatability within 10 nm (see SI) for the thickest film deposition (0 sccm, 2000 s). The films show a maximum roughness of around 3 nm. Taking all measured thicknesses measured using ellipsometry and profilometer, we find a consistent level within a 95% agreement. No substantial variation of the thickness is observed for thermally treated and untreated samples (SI, Fig S1). In the interest of simplicity, we

focus our discussion for the remainder of this paper on films evaporated for 1500 s, nevertheless, our findings are equally valid for other deposition times, which are summarized in the supplementary information, where an overall summary is provided. The stark contrast in obtainable ITO material properties discussed further below can even be qualitatively seen (Fig. 2b) and hints towards a strong ability to engineer the material properties. Four replicated samples are deposited for each experimental condition (i.e. Oxygen flow-rate, deposition time). The repeatability of the process is ensured by the concurrent low variability of the thickness and optical constants (well below 5%). A qualitative analysis on the film colorizations provides first insights on the doping type of the material[46]; a tendency to a brown color (Fig. 2bi, ii) indicates a higher Sn-In doping while a green-yellow colorization corresponds to the presence of oxygen vacancies (Fig. 2biv, v). An overall tendency to a greener colorization of the annealed films with respect to non-annealed ones, is not due to a thickness variation, as one might think, but to the excess number of oxygen vacancies rather than Sn-In dopants. This is due to the annealing process, performed in a chamber filled with H_2 and N_2 at 350 °C, which activates the otherwise quiescent oxygen vacancies. This is further corroborated by a significant thickness difference between annealed and not annealed films (SI, Fig. S1). However, to quantitative analyze the optical constants, spectroscopic ellipsometry studies are reported in Fig. 2ci–v for 1500 s deposition time. Beside 0 sccm, it appears that ITO films not subjected to an annealing process, films are predominantly not absorptive above 500 nm. In the wavelength range from 500 nm to 1680 nm, values of extinction coefficient are, in fact, below hundredths. A major effect attributed to thermal annealing is in fact the activation of the carrier[34], which is responsible of the optical absorption. Because of that, films sputtered at 0 sccm oxygen flow rate (Fig. 2ci) appear to be strongly absorptive in this region, due to the higher oxygen vacancies and consequent higher carrier concentration. Films deposited with this oxygen flow-rate could be embedded in NIR perfect absorbers[47] or as a building block in meatasurface[48]. Consistently, for all the different oxygen flow-rates tested, after annealing, ITO thin films appear to be more absorptive. The value of κ, the imaginary part of the refractive index, of annealed samples substantially increases as a function of the wavelength in the IR region, compared to not annealed samples, thus producing a shift in the plasma frequency and an overall variation of the refractive index, being $n(\omega)$ and $\kappa(\omega)$ in Kramer-Kronig relation. The filling of the oxygen vacancies at 5 and 10 sccm (Fig. 2ciii–iv) induces the sputtered ITO films to show the lowest κ among the other groups, due to the partly filled vacancies and they might be a viable option for low-loss conductive transport layer in optoelectronic devices or as a sensing platform[41]. For higher oxygen flow rate (20, 30 sccm) the films become more absorptive in the IR.

Post-deposition annealing profoundly changes the structural and optical properties of ITO thin films, as previously discussed in the optical characterization. This process, in fact, represents an effective way to promote crystallinity and modify the physical features of ITO films, such as roughness, but also it contributes in drastically altering the carrier distribution. Our ellipsometry studies use a fitting approach, which contemporary minimize the error (RMS) computed in the fitting and considers a graded variation of optical/electrical parameters. This approach is essential for quantitatively pointing out that the resistivity, for annealed samples, is a function of the film depth as discussed below, which confirms that the thermal processes can favor the redistribution of carriers, homogenizing them throughout the sample, as illustrated by Buchanan *et al.*[49]. Another effect, which can be ascribed to thermal heating, is related to optical absorption. Moreover, for oxygen flow-rates above 0 sccm, the absorption significantly increases in the IR region. As an obvious influence on the resistivity, this type of films display an exponential decaying resistivity within the film depth (Fig. 3b, c). Interestingly, the absorption and resistivity trend for films sputtered with a null Oxygen flow-rate (Fig. 3a) have the highest value confined in the film core and it is significantly smaller (1 order of magnitude) than the highest resistivity recorded for the ITO film sputtered at 10 sccm oxygen flow-rate[40]. We can speculate that being the thickest (approx. 600 nm) among the studied groups, the annealing time is not sufficient to completely redistribute the carriers throughout its depth. In details, it is worth mentioning that, considering the thermal gradient (bottom to top) present in the process, due to set-up configuration and presence of the substrate, the annealing time might have not been enough to distribute the carriers within the significantly thicker film (x2), like in the other cases. Nevertheless, this modelling accounts for differences in resistivity within the thickness of the material, and in the 0-sccm films, the difference between the highest and lowest resistance slices is 20 times smaller than others and it is almost negligible.

Effects of the Oxygen Flow Rate and Thermal Treatment on the Electrical Properties

Electrical properties, carrier concentration and mobility of ITO have been found previously to vary for different deposition techniques, but also for different process conditions for the deposition such as power, oxygen flow, and annealing temperature[3,34,35,41]. In this section we focus on the impact of the oxygen flow-rate and thermal post deposition treatment on the electrical properties of ITO. Figure 4 summarizes the electrical properties of the ITO films sputtered with different oxygen flow rate (1500 s), for thermally untreated (a) and treated samples (b), measured using three different methods, i.e. Hall measurement, 4-probe and spectroscopic ellipsometry. It is worth noticing that the measurements (direct and indirect) are in quasi-perfect agreement ($>$ 90% correlation). Only in case of the 4-probe measurement of non-annealed samples, the resistivity has a different trend. This can be attributed to the instability of the contacts-to-film junction, due to the rather soft upper layer of the samples, when not thermally treated. It is evident that not annealed thin films are less conductive, displaying one order of magnitude higher resistivity (a-b), an overall slightly higher mobility (c), lower carrier concentration (d) compared to the annealed samples. Therefore, annealed films are generally more suitable for the implementation of capacitive sensors, and promote the absorption in the optical telecom wavelength, enabling the fabrication of efficient electro-absorption modulators based on ITO films. As previously mentioned, for ITO, electrons are the majority carriers and they are originating mainly from the doping donor Sn and oxygen vacancies. For our sputtering conditions we show that increasing oxygen flow-rate produces an initial increase of the resistivity, induced by a lower carrier concentration. The lower carrier concentration is reached for Oxygen flow rates within 5–20 sccm. Therefore, increasing the oxygen flow rate replenishes the oxygen vacancies up to 10 sccm. For higher

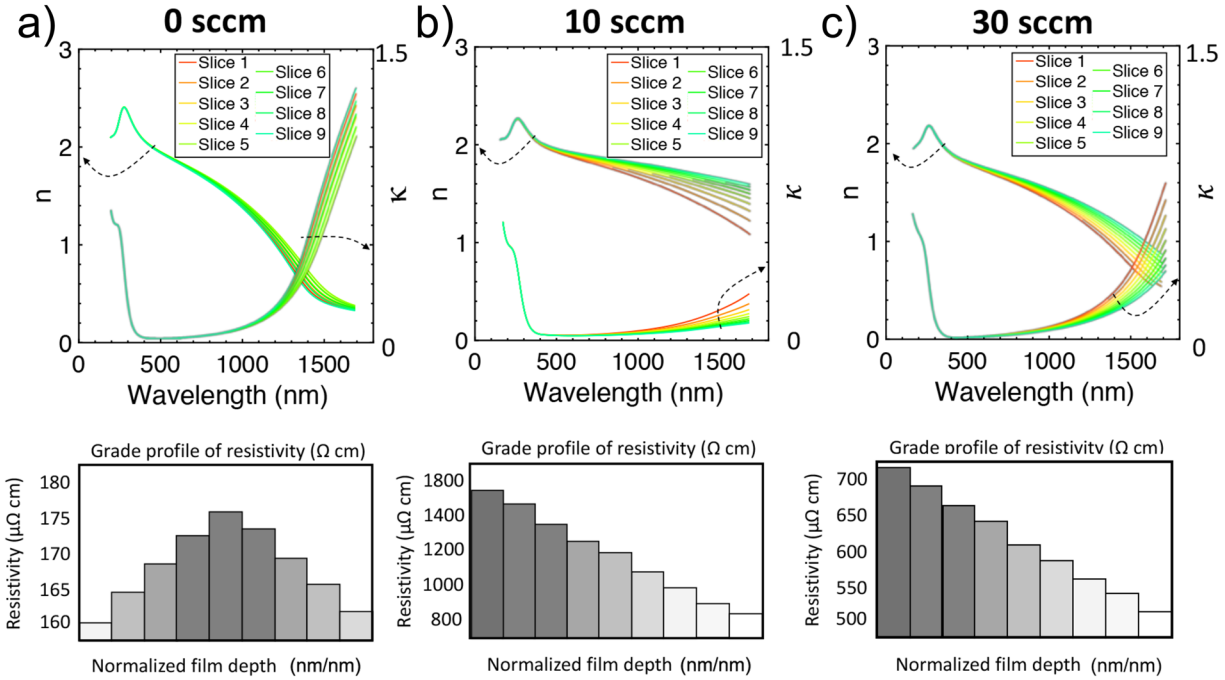

Figure 3. Complex refractive index and resisitivity depth profile (**a**–**c**) Real (left y-axis) and imaginary part (right y-axis) of the refractive index spectral response investigated by ellipsometry. Different curves (red to green) represent different depth profile distribution within the film thickness (red/top layer, green/bottom layer) for 0 (**a**), 10 (**b**), 30 (**c**) sccm after annealing. Bottom row represents the resistivity depth profile along the film thickness. The thickness of the 3 films, (**a**) 600 nm, (**b**) 300 nm, (**c**) 180 nm, on the (x-axis) is normalized for an easy comparison.

oxygen flow-rates the sputtered particles from the target cannot oxidize sufficiently, hence the ITO films are anoxic and sub-oxides such as InO_x and SnO_x are present in the films[45].

For annealed samples both the carrier concentrations and mobility overall decrease by increasing oxygen flow rates[50]. This can be attributed to the concurrent filling of the oxygen vacancies and the deactivation of the Sn donor by the overflowing oxygen. It can be said that 10 sccm of oxygen flow rate can be an optimum for obtaining a high resistivity (low carrier concentration, $\sim 1 \times 10^{19}$) and as previously shown low absorption, satisfactory condition for electro-optic modulators[25,51]. The mobility on the effect of annealing is within the same order of magnitude, although the trend is rather different. The mobility in non-annealed films is higher than for lower carrier concentrations, while the opposite trend is visible for annealed films.

Afterwards, for annealed samples, we investigate the variation of spectral response of the real part of the permittivity (ε') for different oxygen flow-rate and deposition time. The x-intercept of the curve reveals the wavelength where $\varepsilon' = 0$, i.e. ENZ (see SI). The trend of ENZ position as function of the oxygen flow-rate is strongly inherited from the resistivity response (Fig. 5b), displaying a 96% cross correlation. This is further illustrated by the difference scattering time t, which has complementary trend with respect to the ε'' as a function of deposition time and oxygen flow-rate. Our ability, to methodically tune the ENZ position across a broad range of wavelengths from the E- to L-bands (1400 to 2500 nm) offers to engineer precise ENZ-based devices at targeted wavelengths (Fig. 5d). Considering 1500 s deposition time, the longest wavelength reached is for 10 sccm, which corresponds to lower absorption, as well as higher resistivity. As a matter of fact, this further degree of freedom in setting the ENZ position could for instance enables the realization of sub-wavelength electo-optic modulators based on ITO films embedded in integrated photonics circuit[13,15,25,51]. Through this study, RF-sputtered ITO films with crafty ENZ positioning in the optical telecom range can be deposited, thus lowering the energy required to switch from ENZ (high absorption) and epsilon-far-from-zero (low absorption)[52]. An intriguing field that could greatly benefit of this study is metatronics, allowing the implementation of nano-optical circuit entirely based on ITO film, wisely doped, using suitable process parameters[48]. For illustrating the potentiality of this study, we hereby demonstrate the possibility to finely tune RF sputtering parameters to achieve a metatronics circuits based on ITO with opportunity tailored permittivity using the previously discussed process parameters. Therefore, we combine experimental data related to ENZ position with numerical approaches. For a homogeneous thickness of ITO with tailored values of real and imaginary part of the dielectric constant one can design optical lumped-circuit elements in an integrated system. For instance, using a similar approach proposed by Engheta *et al.* in[31,53,54], we design and analyze a nanophotonic circuit based on our ITO films, whose permittivity is function of the oxygen flow-rate used for deposition. It is possible to use sub-wavelength photonic circuit based on different ITO film, sputtered at different oxygen flow-rate, for interacting with a propagating mode (Fig. 6). A $\lambda = 1550$ nm TE_{10} mode is launched in a Silicon waveguide with a permittivity of 12. Our proof-of-principle metatronic circuit is comprised of two ITO-based nanostructures positioned in the center of the waveguide, in

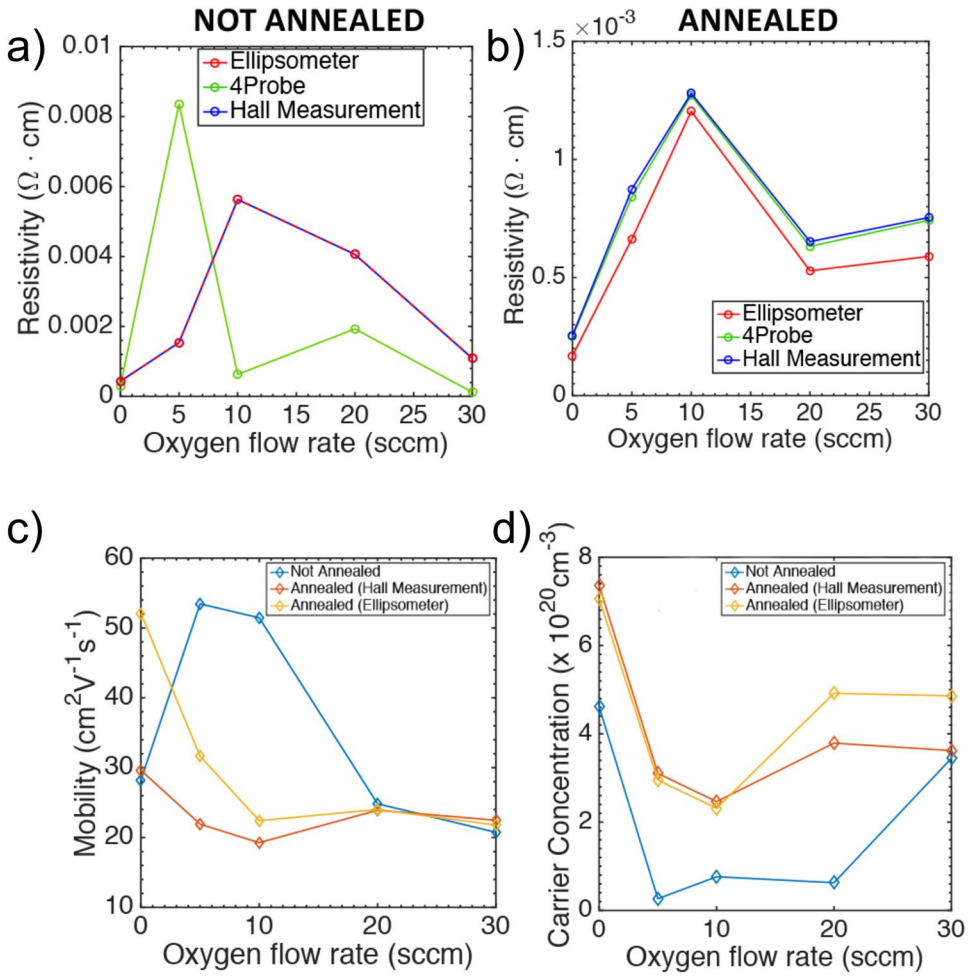

Figure 4. Resistivity measured with different techniques (Ellipsometer, 4-Probe and Hall Measurement) as function of the Oxygen flow-rate thermally untreated (**a**) and treated **(b)** samples. (**c**) Mobility and (**d**) carrier concentration for treated and untreated samples validated through direct (Hall Effect) and indirect (ellipsometer) measurement.

two possible configurations (parallel/series). The thickness, t, of the ITO films is 50 nm, thus a lumped circuit model can be applied, being $t \ll \lambda$. In the equivalent circuit, the film with real part of the permittivity (ε') larger than zero acts as a capacitor, whereas the film with negative real part as an inductor. The films are also characterized by a damping ($\varepsilon'' > 0$), which induces losses, modeled in the lumped model as a resistance. A capacitor-like ITO film can be sputtered adopting a null oxygen flow-rate, obtaining an ENZ position shifted towards red with respect to the considered wavelength (1550 nm), while an inductor can be obtained using 20 sccm oxygen flow-rate, resulting into a blue shift of the ENZ position. When the films with ε' with opposite signs are placed in parallel configuration (Fig. 6a), there is a pronounced impedance mismatch, leading to a high reflection coefficient, which translates to a -12 dB transmission of the signal. Contrarily, for films placed in series (Fig. 6b) the imaginary part of the permittivity becomes negligible and only insertion losses are present, achieving a transmission of -4 dB. Based on our previous work on ITO-based electrooptic modulators[13,25] our future work includes actively reconfigured metatronic circuit building blocks on-chip using our ITO film control.

Discussion

Understanding the effect of process parameters for tailoring ITO films electro-optical properties is crucial for both optimizing device performances such as in optics, electronics, or plasmonics, but also enables new material-platforms to realize metatronic circuits. In this study, we mapped the dependency of oxygen flow-rate and thermal annealing on the structural, optical, and electrical properties of the ITO thin films deposited by RF sputtering. We derive the function which regulates the deposition rate of ITO as function the oxygen flow-rate. By altering the mean free path and gas current of null ion in the deposition chamber, an increased oxygen flow rate contributes in exponentially decreasing the film thickness. As previously reported[41], for thermally treated samples, we observe an overall increased absorption coefficient (κ), a 6-folds lower resistivity and significantly higher carrier concentration ($\sim 8 \times 10^{20}$ cm^{-3}). For a fixed deposition time, by tuning the oxygen flow rate, we modify the number of oxygen vacancies in the film, and after activation through thermal treatment, we manage to control the absorption and the carrier concentration of the film. Increasing oxygen flow-rate (up to 20 sccm) reduces the oxygen vacancies in ITO, which in turn results in a decrease

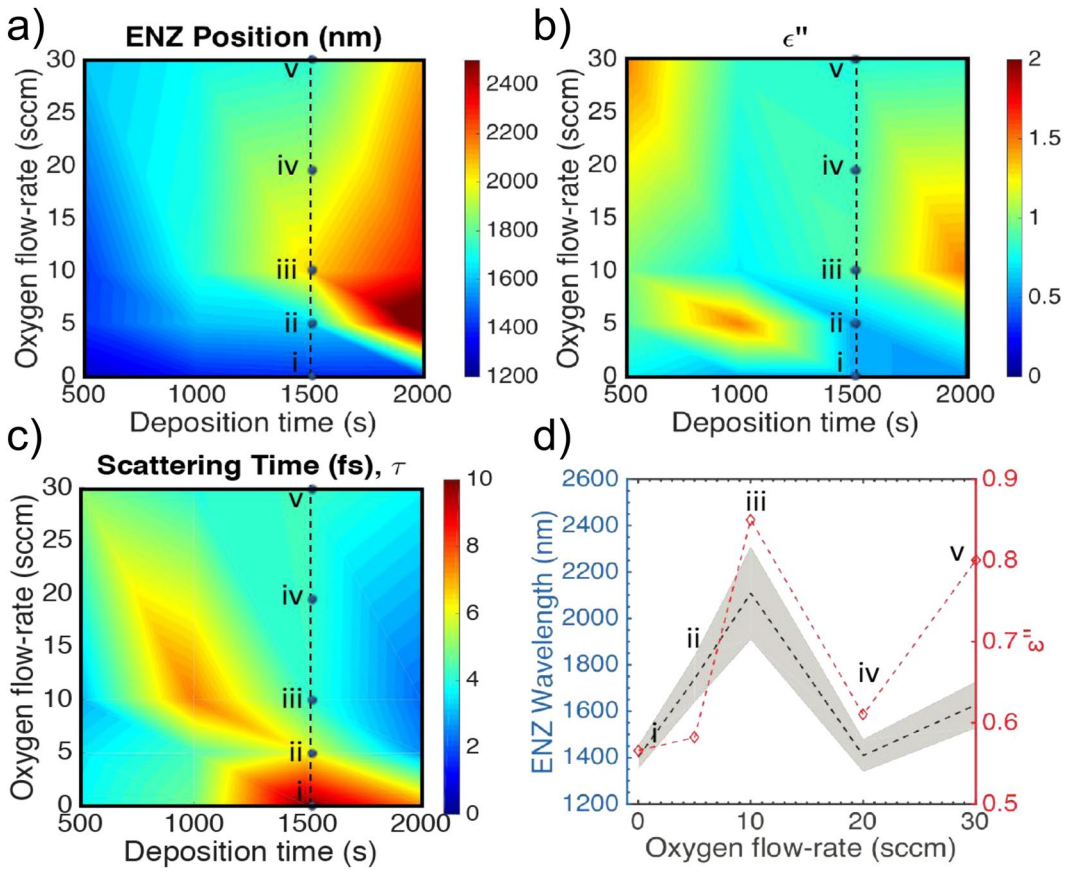

Figure 5. Experimental (interpolated) data of ITO film loss and ENZ-position as a function of oxygen process flow-rate. (**a**) Measured ENZ wavelength as function of the deposition time and oxygen flow-rate. (**b**) Measured damping (ε'') function of the deposition time and oxygen flow-rate. (**c**) Scattering Time t as function of the deposition time and oxygen flow-rate. (**d**) ENZ wavelength (black dashed line, left-axis) as function of the Oxygen flow-rate and corresponding damping (ε'') (red dashed line, right-axis) for ITO film deposited for 1500 s.

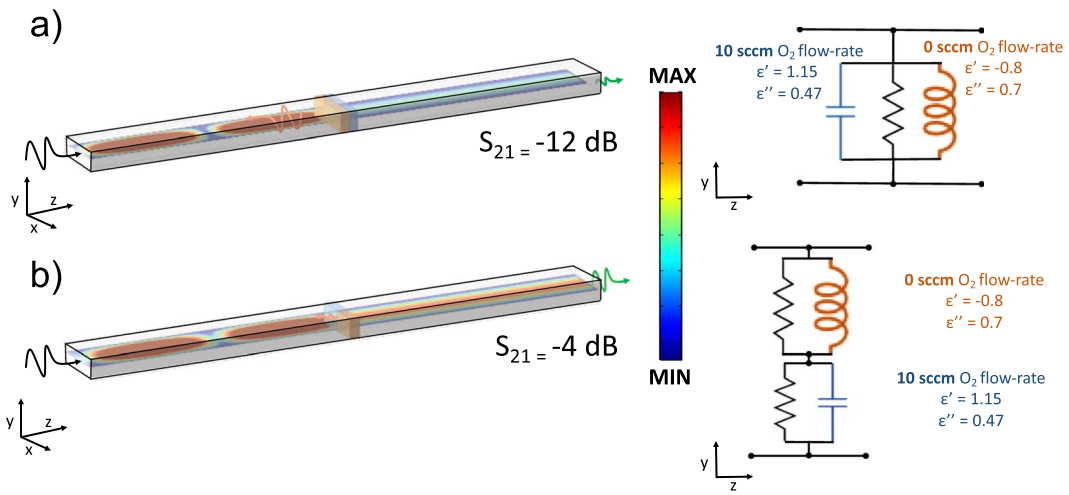

Figure 6. 3D view of the numerical simulation of a metatronics parallel and series setup. A TE_{10} incident mode is propagating in a waveguide ($\varepsilon = 12$). Two ITO film in parallel a and series b configuration are placed in between of the waveguide. Color map of the simulation results for the normalized electric field intensity distributions for the series (**a**) and parallel (**b**). The transmission coefficients (S_{21}) along with the equivalent circuit model and the process parameters used for obtaining specific permittivity values are reported on the right side. $\lambda = 1550$ nm, Silicon waveguide dimensions 500 nm by 220 nm. ITO film thicknesses are 50 nm.

of the carrier mobility by a factor of 2 and carrier concentration by 5-fold, significantly diminishing the resistance and optical absorption. Comparatively to DC sputtered film[44], for which the maximum resistivity was found to be 1.56×10^{-3} Ω-cm at 30 sccm, here, using an RF-sputtering system we obtain a similar trend, with a peak in resistivity for 10 sccm oxygen flow rate ITO film, which was 10 times larger than the one obtained in null oxygen flow rate conditions. For oxygen flow rate greater than 20 sccm, the presence of SnO_2 produces *n* doping of the lattice, adding electrons to the conduction band, giving rise to a lowered resistivity[45] and optical losses with respect to 10 sccm. X-ray diffraction pattern and elemental analysis could be used in the following studies to substantiate our findings in terms of dopants and variation of lattice distances.

Corroborated with modeling of the spectral response of the ITO films, we precisely derive the resistivity and complex optical constant of annealed samples as function of the film depth, using a multi-layered fitting approach. We find that our thermal annealing process can redistribute the carrier concentration, as a function of the thermal gradient applied and initial carrier concentration. The film deposited with 10 sccm oxygen flow rate presents the largest sweep throughout its depth, with a resistivity that varies from ~1600 μΩ. cm to ~600 μΩ. cm and κ from 0.1 to 0.2. This finding can be exploited for better modelling and interpreting experimental results of ITO-based active plasmonic modulators, which are particularly sensitive to the surrounding dielectric environment, or for fabricating graded optical devices.

We extend our study for different deposition time conditions, aiming for mapping the ENZ position, damping and scattering time as function of oxygen flow-rate with deposition time. Ultimately, in annealed samples we found that the ENZ point reaches a maximum wavelength, which red-shifts from 1.4 to 2.1 μm for 10 sccm oxygen flow-rate only to blue-shift for higher oxygen concentration in the chamber, maintaining a similar trend with respect to the resistivity. Using these process parameters, we forced the ENZ position to be at shorter wavelength compared to the mid-IR region reported by Wang *et al.*[23], enabling for ENZ-based applications in the telecommunication wavelength (C-band), such as elctro-absorption modulators, plasmonic absorbers and nonlinear devices. Exploiting these results, we simulate a sub-wavelength metatronic circuit based on ITO films, placed in the center of a waveguide, which exhibit tailored permittivity according to specific oxygen flow-rate. We demonstrated the possibility to use a lumped circuit entirely based on ITO as a sub-wavelength filter, for example, at 1550 nm in an integrated photonic circuit.

In conclusion, in this novel study, we demonstrated the ability to accurately tune the electrical and optical properties of ITO films in a wide range of frequency ranging from VIS to IR. We thence show a precise control over conductivity, carrier density, and mobility of the ITO films enabled by tailoring of process parameters, such as oxygen flow rate, deposition time and post-deposition thermal treatment, assessed thorough a rigorous cross-validation procedure. By controlling the oxygen flow ratio during sputtering, oxygen vacancies could be filled, making it possible to prepare optimal ITO films that exhibited suitable electrical performance, while still preserving optical transparency in a wide range of frequencies. Following this approach, we demonstrate a fabricability and repeatability of epsilon-near-zero (ENZ) on-chip platforms. We anticipate these findings to enable a plurality of functional devices for fields to include opto-electronics, plasmonics, metasurfaces, and possibly most novel, to metatronics. Using this rigorous material control, we finally provide an example showing the ability to engineer a metatronic-based sub-wavelength building block demonstrating an optical switch.

Methods

RF Deposition. ITO ultra-thin films were deposited on a cleaned Si substrate with a nominal 300 nm SiO_2 on it (1 cm × 1 cm) at 313 K by reactive RF sputtering using Denton Vacuum Discovery 550 Sputtering System. They were prepared with the same time which is 1500 seconds. The target is consisting of 10% SnO_2 and 90% In_2O_3 by weight. The ITO films were prepared with the same Argon flow-rate which is 40 sccm and different oxygen flow-rates which are 0 sccm, 5 sccm, 10 sccm, 20 sccm, and 30 sccm respectively. All the deposition time is 1500 s. There are four chips for each group. Two of them are tapped for later profilometer measurement. The vacuum setpoint is 5 Torr before deposition and the target will be pre-sputtered with the same deposition condition for 120 s to remove the surface oxide layer of the target to avoid the contamination of the films. RF voltages were 300 voltage and RF bias were 25 voltage. After all parameters reached their set-points, deposition began.

Annealing process. After deposition, few samples were annealed in a sealed chamber filled with H_2 and N_2 to avoid the influence of oxygen in the air during the annealing process at 350 °C for 15 mins. The thin film is in direct contact with the cover, while the substrate touches the bottom holder, leading to a thermal gradient top (cold) to bottom (hot).

Ellipsometry. We carried out spectroscopic ellipsometry measurement using J.A. Woollam M-2000 DI, which covered wavelength from 200 nm to 1680 nm. Analysis of the data used the corresponding CompleteEASE to extract thickness, complex optical constants, and other electrical parameters. Silicon substrate and a nominal 300 nm silicon dioxide layer were also considered in ITO fitting model since, being commercial products, the related information was not exhaustive for analysis. We first fit the transparent region using Cauchy model to find out the closest thickness value for ITO thin film and fix it. Then we fitted the data using B-spline model and subsequently we expanded the fitting region from transparent region to the entire wavelength region. After that we re-parameterized the data using different oscillators in GenOsc, i.e. Drude, Cauchy-Lorentz and Lorentz oscillators. More details on the fitting model are provided in the SI.

Resistance measurement. The resistivity and Hall voltages (Ecopia HMS-5500 Hall Effect measurement) of the films were measured using 4-terminal van der Pauw geometry. The electric contacts were at the corners of a 1 × 1 cm sample of the film to be investigated. Electrical measurements were used for defining the thin film sheet resistance, carrier concentration and mobility.

References

1. Huang, L. & Zhong, J. Z. Indium tin oxide (ITO) layer forming. United States patent US8049862B2 (November 1, 2011).
2. Gwamuri, J., Marikkannan, M., Mayandi, J., Bowen, P. K. & Pearce, J. M. Influence of Oxygen Concentration on the Performance of Ultra-Thin RF Magnetron Sputter Deposited Indium Tin Oxide Films as a Top Electrode for Photovoltaic Devices. *Materials (Basel)* **9** (2016).
3. Chityuttakan, C., Chinvetkitvanich, P., Chatraphorn, S. & Chatraphorn, S. Influence of deposition parameters on the quality of ITO films for photovoltaic application, 3 (n.d.).
4. Qin, F. *et al*. Indium tin oxide (ITO)-free, top-illuminated, flexible perovskite solar cells. *J. Mater. Chem. A* **4**, 14017–14024 (2016).
5. Ho, W.-J., Sue, R.-S., Lin, J.-C., Syu, H.-J. & Lin, C.-F. Optical and Electrical Performance of MOS-Structure Silicon Solar Cells with Antireflective Transparent ITO and Plasmonic Indium Nanoparticles under Applied Bias Voltage. *Materials* **9**, 682 (2016).
6. Linnet, J. *et al*. Transparent and conductive electrodes by large-scale nano-structuring of noble metal thin-films. *Opt. Mater. Express, OME* **8**, 1733–1746 (2018).
7. Li, E., Gao, Q., Chen, R. T. & Wang, A. X. Ultracompact Silicon-Conductive Oxide Nanocavity Modulator with 0.02 Lambda-Cubic Active Volume. *Nano Lett.* **18**, 1075–1081 (2018).
8. Abdelatty, M. Y., Badr, M. M. & Swillam, M. A. Compact Silicon Electro-Optical Modulator Using Hybrid ITO Tri-Coupled Waveguides. *J. Lightwave Technol., JLT* **36**, 4198–4204 (2018).
9. Yang, J. *et al*. A flexible and high-performance all-solid-state supercapacitor device based on Ni3S2 nanosheets coated ITO nanowire arrays on carbon fabrics. *RSC Adv.* **6**, 75186–75193 (2016).
10. Knickerbocker, S. A. & Kulkarni, A. K. Calculation of the figure of merit for indium tin oxide films based on basic theory. *Journal of Vacuum Science & Technology A: Vacuum, Surfaces, and Films* **13**, 1048–1052 (1995).
11. Roozeboom, F. *Silicon Compatible Materials*, *Processes*, *and Technologies for Advanced Integrated Circuits and Emerging Applications* (The Electrochemical Society, 2011).
12. Feigenbaum, E., Diest, K. & Atwater, H. A. Unity-Order Index Change in Transparent Conducting Oxides at Visible Frequencies. *Nano Lett.* **10**, 2111–2116 (2010).
13. Sorger, V. J., Lanzillotti-Kimura, N. D., Ma, R.-M. & Zhang, X. Ultra-compact silicon nanophotonic modulator with broadband response. *Nanophotonics* **1**, 17–22 (2012).
14. Zhao, H., Wang, Y., Capretti, A., Negro, L. D. & Klamkin, J. Silicon photonic modulators based on epsilon-near-zero indium tin oxide materials. In *2014 IEEE Photonics Conference*, pp. 334–335 (2014).
15. Vasudev, A. P., Kang, J.-H., Park, J., Liu, X. & Brongersma, M. L. Electro-optical modulation of a silicon waveguide with an epsilon-near-zero material. *Opt. Express, OE* **21**, 26387–26397 (2013).
16. Ye, C., Khan, S., Li, Z. R., Simsek, E. & Sorger, V. J. λ-Size ITO and Graphene-Based Electro-Optic Modulators on SOI. *IEEE Journal of Selected Topics in Quantum Electronics* **20**, 40–49 (2014).
17. Melikyan, A. *et al*. Surface plasmon polariton absorption modulator. *Opt. Express, OE* **19**, 8855–8869 (2011).
18. Abdelatty, M. Y., Badr, M. M. & Swillam, M. A. Hybrid plasmonic electro-optical absorption modulator based on epsilon-near-zero characteristics of ITO. In *Integrated Optics: Devices*, *Materials*, *and Technologies XXII*, Vol. 10535, p. 105351T (International Society for Optics and Photonics, 2018).
19. Babicheva, V. E., Boltasseva, A. & Lavrinenko, A. V. Transparent conducting oxides for electro-optical plasmonic modulators. *Nanophotonics* **4**, 165–185 (2015).
20. Shi, K., Haque, R. R., Zhao, B., Zhao, R. & Lu, Z. Broadband electro-optical modulator based on transparent conducting oxide. *Opt. Lett., OL* **39**, 4978–4981 (2014).
21. Huang, Y.-W. *et al*. Gate-Tunable Conducting Oxide Metasurfaces. *Nano Lett.* **16**, 5319–5325 (2016).
22. Lee, H. W. *et al*. Nanoscale Conducting Oxide PlasMOStor. *Nano Letters* **14**, 6463–6468 (2014).
23. Wang, Y. *et al*. Tunability of indium tin oxide materials for mid-infrared plasmonics applications. *Opt. Mater. Express, OME* **7**, 2727–2739 (2017).
24. Amin, R. *et al*. Low-loss tunable 1D ITO-slot photonic crystal nanobeam cavity. *Journal of Optics* **20**, 054003 (2018).
25. Amin, R. *et al*. 0.52 V mm ITO-based Mach-Zehnder modulator in silicon photonics. *APL Photonics* **3**, 126104 (2018).
26. Ma, Z., Li, Z., Liu, K., Ye, C. & Sorger, V. J. Indium-Tin-Oxide for High-performance Electro-optic Modulation. *Nanophotonics* **4**, 198–213 (2015).
27. Amin, R. *et al*. A deterministic guide for material and mode dependence of on-chip electro-optic modulator performance. *Solid-State Electronics* **136**, 92–101 (2017).
28. Amin, R. *et al*. Active material, optical mode and cavity impact on nanoscale electro-optic modulation performance. *Nanophotonics* **7**, 455–472 (2018).
29. Liberal, I., Mahmoud, A. M., Li, Y., Edwards, B. & Engheta, N. Photonic doping of epsilon-near-zero media. *Science* **355**, 1058–1062 (2017).
30. Alam, M. Z., Leon, I. D. & Boyd, R. W. Large optical nonlinearity of indium tin oxide in its epsilon-near-zero region. *Science* **352**, 795–797 (2016).
31. Li, Y., Liberal, I., Giovampaola, C. D. & Engheta, N. Waveguide metatronics: Lumped circuitry based on structural dispersion. *Sci Adv* **2** (2016).
32. Park, Y.-C., Kim, Y.-S., Seo, H.-K., Ansari, S. G. & Shin, H.-S. ITO thin films deposited at different oxygen flow rates on Si(100) using the PEMOCVD method. *Surface and Coatings Technology* **161**, 62–69 (2002).
33. Meng, L.-J., Gao, J., Silva, R. A. & Song, S. Effect of the oxygen flow on the properties of ITO thin films deposited by ion beam assisted deposition (IBAD). *Thin Solid Films* **516**, 5454–5459 (2008).
34. Guillén, C. & Herrero, J. Structure, optical, and electrical properties of indium tin oxide thin films prepared by sputtering at room temperature and annealed in air or nitrogen. *Journal of Applied Physics* **101**, 073514 (2007).
35. Guillén, C. & Herrero, J. Influence of oxygen in the deposition and annealing atmosphere on the characteristics of ITO thin films prepared by sputtering at room temperature. *Vacuum* **80**, 615–620 (2006).
36. Kerkache, L., Layadi, A., Dogheche, E. & Rémiens, D. Physical properties of RF sputtered ITO thin films and annealing effect. *J. Phys. D: Appl. Phys.* **39**, 184 (2006).
37. Dao, V. A. *et al*. rf-Magnetron sputtered ITO thin films for improved heterojunction solar cell applications. *Current Applied Physics* **10**, S506–S509 (2010).
38. Terzini, E., Thilakan, P. & Minarini, C. Properties of ITO thin films deposited by RF magnetron sputtering at elevated substrate temperature. *Materials Science and Engineering: B* **77**, 110–114 (2000).
39. Akkad, F. E., Marafi, M., Punnoose, A. & Prabu, G. Effect of Substrate Temperature on the Structural, Electrical and Optical Properties of ITO Films Prepared by RF Magnetron Sputtering. *physica status solidi (a)* **177**, 445–452 (2000).
40. Tuna, O., Selamet, Y., Aygun, G. & Ozyuzer, L. High quality ITO thin films grown by dc and RF sputtering without oxygen. *J. Phys. D: Appl. Phys.* **43**, 055402 (2010).
41. Hu, Y., Diao, X., Wang, C., Hao, W. & Wang, T. Effects of heat treatment on properties of ITO films prepared by rf magnetron sputtering. *Vacuum* **75**, 183–188 (2004).
42. Solieman, A. & Aegerter, M. A. Modeling of optical and electrical properties of In2O3:Sn coatings made by various techniques. *Thin Solid Films* **502**, 205–211 (2006).

43. Chiang, J.-L., Jhan, S.-S., Hsieh, S.-C. & Huang, A.-L. Hydrogen ion sensors based on indium tin oxide thin film using radio frequency sputtering system. *Thin Solid Films* **17**, 4805–4809 (2009).
44. Tien, C.-L., Lin, H.-Y., Chang, C.-K. & Tang, C.-J. Effect of Oxygen Flow Rate on the Optical, Electrical, and Mechanical Properties of DC Sputtering ITO Thin Films, https://www.hindawi.com/journals/acmp/2018/2647282/.
45. Li, S., Qiao, X. & Chen, J. Effects of oxygen flow on the properties of indium tin oxide films. *Materials Chemistry and Physics* **98**, 144–147 (2006).
46. Materion Inc, Transparent Conductive Oxide Thin Films, (n.d.).
47. Xue, C. *et al*. Wide-angle Spectrally Selective Perfect Absorber by Utilizing Dispersionless Tamm Plasmon Polaritons. *Scientific Reports* **6**, 39418 (2016).
48. Forouzmand, A., Salary, M. M., Inampudi, S. & Mosallaei, H. A Tunable Multigate Indium-Tin-Oxide-Assisted All-Dielectric Metasurface. *Advanced Optical Materials* **6**, 1701275 (2018).
49. Buchanan, M., Webb, J. B. & Williams, D. F. Preparation of conducting and transparent thin films of tin-doped indium oxide by magnetron sputtering. *Appl. Phys. Lett.* **37**, 213–215 (1980).
50. Lee, H.-C. & Park, O. O. Behaviors of carrier concentrations and mobilities in indium–tin oxide thin films by DC magnetron sputtering at various oxygen flow rates. *Vacuum* **77**, 69–77 (2004).
51. Tahersima, M. H. *et al*. Coupling-controlled Dual ITO Layer Electro-Optic Modulator in Silicon Photonics, 13 (n.d.).
52. Lu, Z., Zhao, W. & Shi, K. Ultracompact Electroabsorption Modulators Based on Tunable Epsilon-Near-Zero-Slot Waveguides. *IEEE Photonics Journal* **4**, 735–740 (2012).
53. Engheta, N., Salandrino, A. & Alù, A. Circuit Elements at Optical Frequencies: Nanoinductors, Nanocapacitors, and Nanoresistors. *Physical Review Letters* **95** (2005).
54. Alù, A. & Engheta, N. All Optical Metamaterial Circuit Board at the Nanoscale. *Phys. Rev. Lett.* **103**, 143902 (2009).
55. Zhu, S., Lo, G. Q. & Kwong, D. L. Design of an ultra-compact electro-absorption modulator comprised of a deposited TiN/HfO_2/ITO/Cu stack for CMOS backend integration. *Opt. Express* **22**, 17930 (2014).

Acknowledgements

VS is funded by AFOSR (FA9550-17-1-0377) and ARO (W911NF-16-2-0194) and HD by NASA STTR, Phase I (80NSSC18P2146).

Author Contributions

V.S. conceived the original idea and supervised the project. Y.G. fabricated the samples and performed the measurement. M.M. and Z.M. develop the model and carried out the numerical simulations. Y.G. and M.M. processed the experimental data performed the analysis, drafted the manuscript and designed the figures. M.T., S.S. and R.A. and H.D. aided in interpreting the results and worked on the manuscript. All authors discussed the results and commented on the manuscript.

Additional Information

Supplementary information accompanies this paper at https://doi.org/10.1038/s41598-019-47631-5.

Competing Interests: The authors declare no competing interests.

Publisher's note: Springer Nature remains neutral with regard to jurisdictional claims in published maps and institutional affiliations.